THE ASTROPHYSICAL JOURNAL, 438:672–679, 1995 January 10

JOINT *ROSAT–COMPTON GRO* OBSERVATIONS OF THE X-RAY–BRIGHT SEYFERT GALAXY IC 4329A

G. M. MADEJSKI,[1,2] A. A. ZDZIARSKI,[3] T. J. TURNER,[1,2] C. DONE,[4] R. F. MUSHOTZKY,[1] R. C. HARTMAN,[1] N. GEHRELS,[1] A. CONNORS,[5] A. C. FABIAN,[6] K. NANDRA,[6] A. CELOTTI,[6] M. J. REES,[6] W. N. JOHNSON,[7] J. E. GROVE,[7] AND C. H. STARR[1,7,8]

Received 1994 February 14; accepted 1994 July 15

ABSTRACT

We report a simultaneous *ROSAT* and *GRO* observation of the X-ray–bright Seyfert galaxy IC 4329A. For the *GRO* OSSE detector, we also present the sum of the data for this and earlier observations. The overall spectrum is very well described as a power law with an energy spectral index of ~ 1 absorbed at low energies plus a strong Compton reflection component, typical for Seyfert 1 galaxies. The low energy absorption can be well described by a sum of a neutral column density of $\sim 3 \times 10^{21}$ cm^{-2}, most of which is associated with the edge-on galactic disk of IC 4329A, plus an edgelike feature at ~ 700 eV; this feature implies either complex absorption (due to additional ionized material, or due to partial covering), or a soft excess. The data only weakly constrain the presence of a high-energy cutoff in the underlying power law; they are compatible with an exponential cutoff at any energy $E_C \gtrsim 100$ keV. The relative steepness of the OSSE data, with the power-law energy index of 1.6 ± 0.2, can be accounted for entirely by the contribution of the high-energy tail of the reflection component when $E_C \to \infty$. (We find that the definite cutoff at an energy $E_C \sim 130$ keV suggested in the recently published analysis of the OSSE data for this object is due to a data reduction error.) Including nonsimultaneous *Ginga* observations with 2 keV fluxes matching well that of *ROSAT* gives us likely broad-band X-ray/γ-ray spectra of the object from ~ 0.1 keV up to several hundred keV. Joint spectral analysis of the data sets from the three instruments gives results similar to those from *ROSAT*/OSSE only, except that the cutoff energy is now constrained to be at 250 keV $\lesssim E_C \lesssim 1700$ keV. The constraint on E_C markedly distinguishes this object from NGC 4151, where E_C was lower, ~ 50 keV; this has implications for emission models for AGNs as well as for their contribution to the X-ray background.

We also report the *ROSAT* spectrum of the companion object to the Seyfert galaxy, the elliptical galaxy IC 4329 located $\sim 3'$ away. Its spectrum is well described by an optically thin thermal plasma with $kT = 0.9$ keV, with a 0.1–2 keV flux of 8×10^{-13} ergs cm^{-2} s^{-1}, corresponding to a luminosity of $\sim 8 \times 10^{41}$ ergs s^{-1}.

Subject headings: galaxies: individual (IC 4329A, IC 4329) — galaxies: Seyfert — X-rays: galaxies — gamma rays: observations

1. INTRODUCTION

The nature of high-energy emission from AGNs is still not understood. That is due to the lack of sensitivity of instruments at high energies, where good data would constrain theoretical models more tightly. So far, the best studied object has been the one brightest in hard X-rays, NGC 4151. However, we are certain that its X-ray emission is unique as compared to the majority of Seyfert 1's: the 2–20 keV X-ray spectrum of this rather low luminosity object is unusually flat, with a power-law index α (defined via the energy flux $F_E \propto E^{-\alpha}$) of 0.3–0.7 (e.g., Yaqoob et al. 1993), quite different than $\alpha \simeq 0.9$–1, characteristic for the power-law components of bright Seyfert 1's (Pounds et al. 1990; Nandra & Pounds 1994). So, extending any inferences to Seyfert 1's as a class, e.g., with regard to the emission mechanisms or their contribution to the X-ray background, on the basis of the X-ray and soft γ-ray spectrum of NGC 4151 is probably premature and possibly misleading.

The second brightest hard X-ray Seyfert, IC 4329A ($F_{2-10\,\mathrm{keV}} \simeq 2 \times 10^{-10}$ ergs cm^{-2} s^{-1}), is likely to be more representative of Seyfert 1's as a class. It is a relatively nearby ($z = 0.0157$; Wilson & Penston 1979), luminous object. The X-ray spectrum of it is typical for Seyfert 1's, with a power-law component with $\alpha \simeq 1$ (Piro, Yamauchi, & Matsuoka 1990) as well as a component due to reflection of the power law by cold matter (Lightman & White 1988). IC 4329A thus holds a promise to assess the general applicability of theoretical AGN models, e.g., those developed for NGC 4151 (e.g., Zdziarski, Lightman, & Maciołek-Niedźwiecki 1993). We find that the line-of-sight absorption (seen in the *ROSAT* data) due to the host galaxy oriented edge-on is not large enough to affect studies of the X-ray continuum.

X-ray emission in Seyferts is generally variable, and constraining of any models attempting to explain broad-band spectra requires simultaneous observations by several satellites. While in comparison to other Seyferts, IC 4329A varies only modestly, $\pm 50\%$ (Halpern 1982), this variability is strong enough to make simultaneous observations critical for testing theoretical models. To that end, we scheduled our *ROSAT* and *GRO* observations (including those by the OSSE, previously

[1] Laboratory for High Energy Astrophysics, NASA/Goddard, Greenbelt, MD 20771.
[2] With Universities Space Research Association.
[3] N. Copernicus Astronomical Center, Bartycka 18, 00-716 Warsaw, Poland.
[4] The Physics Department, Leicester University, University Road, Leicester LE1 7RH, UK.
[5] Space Science Center, Univ. of New Hampshire, Durham, NH 03824.
[6] Institute of Astronomy, Cambridge University, Madingley Road, Cambridge CB3 0HA, UK.
[7] E. O. Hulburt Center for Space Research, Naval Research Laboratory, Washington, DC 20375.
[8] Also Computer Sciences Corporation.

reported by Fabian et al. 1993, hereafter F93) to be simultaneous. This gives us perhaps the broadest band simultaneous observation of any radio-quiet AGN obtained yet, and we present it below. We find, however, that due to a gap between 2 and 50 keV the confidence regions on spectral parameters are rather large. We can constrain those parameters much more tightly if we use the *Ginga* data (analyzed in Fiore et al. 1992, hereafter F92) that turn out to match the 2 keV *ROSAT* flux very closely. As spectral variations of the object are weak (F92), it is likely that the resulting broadband spectrum is close to a true simultaneous X-ray/γ-ray spectrum of the object.

2. DATA

2.1. *The ROSAT Observation*

The data reported here are from an observation nominally centered at the optical position of IC 4329A, which is at R.A. (2000.0) = $13^h49^m19^s.2$, decl. (2000.0) = $-30°18'34''$. The observation was performed over the period 1993 January 14 11:41–18:46 UT using the *ROSAT* X-Ray Telescope with the PSPC-B in the focal plane, sensitive over 0.1–2.4 keV, with the FWHM energy resolution of $\Delta E/E = 0.43(E_{\rm keV}/0.93)^{-0.5}$. The total on-source exposure time was 8230 s. The data, collected with the spacecraft "wobble" turned on, were processed using the SASS v. 6.2 and PROS v. 2.10. All subsequent spectral fitting used the 1993 January 12 PSPC-B resolution matrix.

The X-ray image of the field containing IC 4329A is shown in Figure 1. IC 4329A is the nearly on-axis (within the $\sim 10'$ nominal *ROSAT* pointing error) source in the PSPC image, at R.A. (2000.0) = $13^h49^m19^s.5$, decl. (2000.0) = $-30°18'27''.3$; its image is consistent with being pointlike Besides IC 4329A, several other sources are present (see Fig. 1), and two show the PSPC count rate greater than 1/100 of that of IC 4329A. The source at $\sim 3'$ away, at R.A. (2000.0) = $13^h49^m5^s.8$, decl. (2000.0) = $-30°17'38''.5$ is within $\sim 10''$ of the optical position of IC 4329, a companion galaxy to IC 4329A, and is likely to be that galaxy indeed. A third source is located about 12′ away, at R.A. (2000.0) = $13^h48^m44^s.5$, decl. (2000.0) = $-30°29'32''.5$ (where the positional error may be slightly larger, $\sim 20''$, due to its off-axis location); we will subsequently call this source S3. We extracted spectra of all three objects from within a 3′ (for IC 4329A and S3) and 1.′6 (for IC 4329) radius circles around the centroid of each source. The background counts corresponding to IC 4329A and S3 were collected from annuli centered on the sources, with inner radius of 5′ and outer radius of 10′, avoiding regions containing any other source. For IC 4329, we selected a background region on the opposite side of IC 4329A, at the same radial distance from it as IC 4329, such that

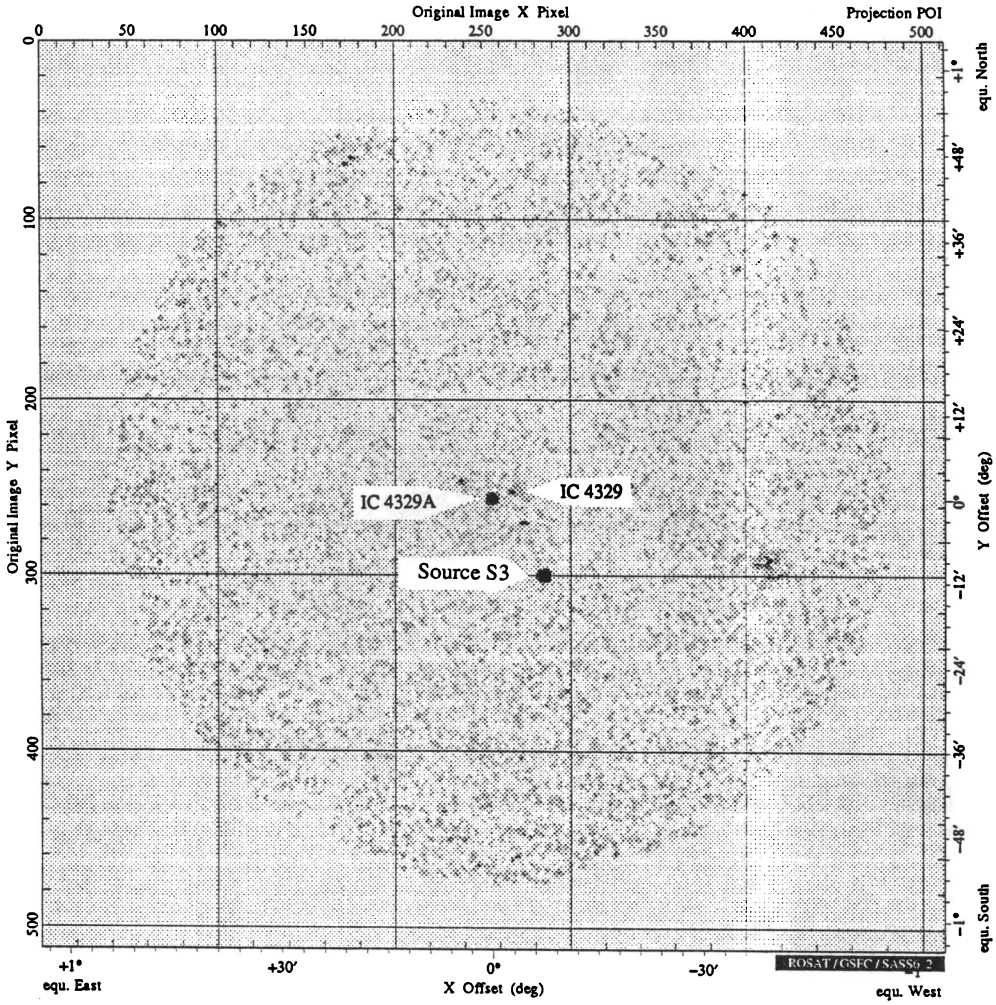

FIG. 1.—The *ROSAT* PSPC image of the field containing IC 4329A and IC 4329

the source and background cells contained the same contamination from the brighter source, such as to subtract away any residual counts due to IC 4329A. The resulting net count rates in the 0.1–2 keV band from IC 4329A, IC 4329, and S3 were, respectively, 2.65 ± 0.02, 0.081 ± 0.004, and 0.086 ± 0.006 counts s^{-1}. To allow for residual PSPC calibration errors, we added in quadrature a systematic error of 2% to the statistical error on the count rate for each channel.

2.2. *The GRO Observations*

IC 4329A was observed by OSSE on the *GRO* during three viewing periods: 41, 1992 October 8–October 15; 44, 1992 November 3–November 17; and 207, 1993 January 12–February 2. The last of these observations (covering the *ROSAT* observation) was described by F93. During this analysis, we have corrected an effective area error in the earlier analysis of the OSSE data, which essentially only affects the conversion of normalization from the count rate to flux. We also have added the data from the earlier 1992 October and 1992 November observations. The observation and analysis techniques for all data were discussed in F93. After correcting the 1993 OSSE data in F93 for a factor of 4 effective area mistake, the results for the combined data as presented here are in agreement with the 1993 data alone. The average OSSE fluxes in the 50–150 keV band for the three periods are 5.7 ± 1.5, 7.4 ± 0.9, and 7.8 ± 0.6, in units of 10^{-4} photons cm^{-2} s^{-1}, for viewing periods, 41, 44, and 207, respectively.

During the 1993 January 12–February 2 *GRO* observing period, the source was also observed by the COMPTEL and EGRET instruments, but it was not detected. The 2 σ COMPTEL upper limits for the viewing period 207 are 7.4, 11, 5.2, and 2.0 in units of 10^{-5} photons cm^{-2} s^{-1} over bands of, respectively, 0.75–1, 1–3, 3–10, and 10–30 MeV. The EGRET 0.1–30 GeV upper limits are 1.6×10^{-7} and 4.9×10^{-8} photons s^{-1} cm^{-2} for the viewing period 207 and for all EGRET observations of this object, respectively.

3. SPECTRAL FITTING

3.1. *Spectrum of IC 4329A*

The main objective of the *ROSAT* part of the coordinated *ROSAT*/*GRO* observations of IC 4329A was to establish the flux level in the soft X-rays. At the time of our joint observations, there were no functioning observatories sensitive in the bandpass between the high-energy cutoff of *ROSAT* and the low-energy cutoff of OSSE, so we compared our data with nonsimultaneous 2–25 keV *Ginga* data. This object was observed for 3 days with *Ginga* in 1989 (Piro et al. 1990; F92), when it was seen to vary by $\sim 25\%$ in flux. Spectral changes, if any, were modest, and all three spectra are consistent with the same spectral shape (F92). Our comparison of *ROSAT* and *Ginga* data revealed that the 2 keV fluxes of the data from 1989 July 8 and 9 are virtually identical with those of *ROSAT*. On the other hand, the *Ginga* flux for 1989 July 10 was about 25% higher. Thus, we used the 1989 July 8, 9 data in joint fits for all three instruments.

3.1.1. *ROSAT Spectrum of IC 4329A*

We present the spectral fits to the *ROSAT* observation alone in Table 1. The data can be adequately described by a simple power law with the best-fit parameters of $\alpha = 0.15 \pm 0.18$, absorbed by a column of $N_H = (2.0 \pm 0.3) \times 10^{21}$ cm^{-2}. (All errors are given for 90% confidence for one parameter of interest, i.e., $\Delta\chi^2 = 2.7$.) The data and residuals are presented in Figure 2. However, even though the χ^2 is acceptable (46.1/33 d.o.f.), inspection of the residuals shows an edgelike feature at ~ 700 eV. Incorporating an edge into the model improves the statistics to $\chi^2 = 30.3/42$ d.o.f., and it gives $\alpha = 0.83 \pm 0.4$, consistent with the spectral index observed by *Ginga*, $\alpha \simeq 1.0$; N_H is now $(3.0 \pm 0.8) \times 10^{21}$ cm^{-2}. The data and residuals for this model are given in Figure 3. The edge energy is $E_{edge} = 0.72 \pm 0.07$ keV, and its optical depth is $\tau_{edge} = 0.56 \pm 0.24$. We discuss the possible instrumental effects on the inferred spectral parameters in the Appendix, but we conclude there that the presence of the feature is independent on these effects.

The energy of the edge is inconsistent with that expected from neutral absorber and implies that it is most likely due to O VI and O VII, which is suggestive of ionized absorber. Therefore, we fitted the data by a power law modified by a sum of neutral and ionized absorbers. We use the XSTAR implementation of the ionized absorber model (with no self-emission), which assumes a single-zone, optically thin, constant density material, where the temperature is calculated self-consistently (cf. Krolik & Kallman 1992; see also Done et al. 1992). The ionization parameter ξ is defined as $L/(nr^2)$, where L is the

TABLE 1

PARAMETERS FOR THE *ROSAT* FITS

Model[a]	N_H (cold) (10^{21} cm^{-2})	α	E_{edge} (keV) (10^{21} cm^{-2})	τ_{edge}	N_H (ionized,[c] or cold partial covering[d])	$\xi^{b,c}$ (or partial covering fraction[d])	Soft Excess (index[e] or blackbody kT [eV][f])	χ^2/d.o.f.
A	2.0 ± 0.3	0.15 ± 0.18	...	...	...	...	...	46.1/44
B	3.0 ± 0.8	0.83 ± 0.4	0.72 ± 0.07	0.56 ± 0.24	...	...	...	30.3/42
C	2.3 ± 0.7	1.0 (fixed)	...	...	$3.8^{+1.4}_{-1.0}$	$3.4^{+22}_{-1.6}$	...	30.4/43
D	$1.8^{+0.6}_{-0.4}$	1.0 (fixed)	...	...	$5.1^{+1.8}_{-0.9}$	$72^{+8}_{-16}\%$	...	32.1/43
E	$5.6^{+1.6}_{-1.1}$	1.0 (fixed)	...	...	...	...	$5.7^{+1.2}_{-0.7}$	32.1/43
F	4.7 ± 0.4	1.0 (fixed)	...	...	...	...	68 ± 10	30.9/43

NOTE.—All errors are given for $\Delta\chi^2 = 2.7$.

[a] The models are A, Power-law with cold absorption; B, Power-law with cold absorption and an edge; C, Power-law with cold absorber plus ionized absorber; D, Power-law with cold absorption plus partial covering by additional cold absorber; E, Power-law with cold absorption plus soft excess (of power-law form); F, Power-law with cold absorption plus soft excess (of blackbody form).

[b] Ionization parameter ξ, as defined in the text.

[c] For Model C.

[d] For Model D.

[e] For Model E.

[f] For Model F.

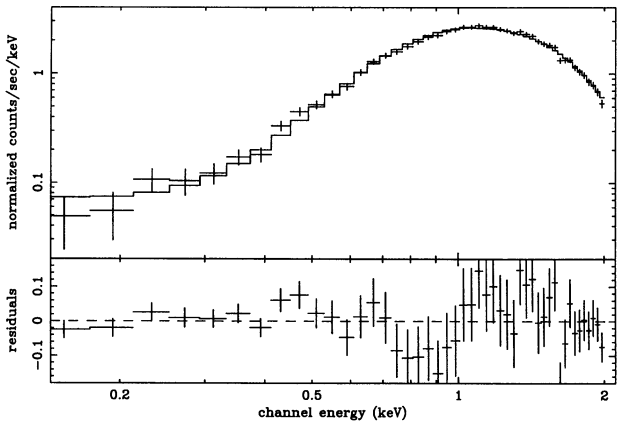

FIG. 2.—The *ROSAT* data for IC 4329A, as fitted to a simple, absorbed power law (*top*) and the resulting residuals (*bottom*). See Table 1 for the model parameters.

ionizing luminosity between 1 and 1000 Ry, r is the distance from the ionizing source, and n is the gas density (cf. Kallman & McCray 1982). In our fit, we assume $\alpha = 1$ and obtain the neutral column of $2.3 \pm 0.7 \times 10^{21}$ cm^{-2}, plus an ionized column of $(3.8^{+1.4}_{-1.0}) \times 10^{21}$ cm^{-2} with the ionization parameter $\xi = 3.4^{+22}_{-1.6}$; χ^2 is now 30.4/43 d.o.f.

However, the ionized absorber model is not a unique interpretation of the spectral complexity present in the *ROSAT* data, due to the modest energy resolution of the PSPC. An alternative acceptable model is partial covering by neutral material, yielding $\chi^2 = 32.1/43$ d.o.f. for the fixed $\alpha = 1$, with $1.8^{+0.6}_{-0.4} \times 10^{21}$ cm^{-2} covering 100% of the source, with an additional column of $5.1^{+1.8}_{-0.9} \times 10^{21}$ cm^{-2} covering $72\%^{+0.6\%}_{-0.4\%}$ of the source. We note here that this column is substantially smaller than the partial absorber column of $\sim 2 \times 10^{24}$ cm^{-2} which was invoked as one alternative (next to Compton reflection) to account for the "hump" above ~ 8 keV reported by Piro et al. (1990) on the basis of the *Ginga* data.

It is also possible that the edgelike feature is due to even higher (than 3×10^{21} cm^{-2}) column of cold absorber, with a soft excess (due to, e.g., a tail end of emission from an accretion disk). The soft excess can be modeled as a blackbody or a power law; fixing the hard power law at $\alpha = 1$ results in $\chi^2 = 30.9/43$ d.o.f. with a blackbody temperature of 68 ± 10 eV and N_H of $4.7 \pm 0.4 \times 10^{21}$ cm^{-2}; a steep power law form of the soft excess (with α_s of 5.0–6.9) is also allowed, but in any case, the intersection with the hard power law must be near 600–700 eV.

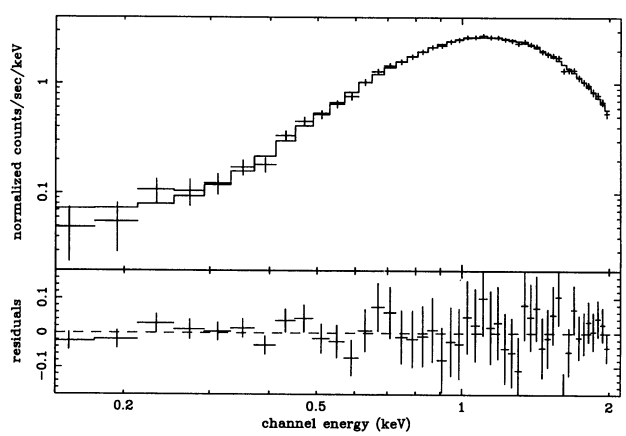

FIG. 3.—The *ROSAT* data for IC 4329A, as fitted to an absorbed power law with an edge at 0.72 keV (*top*) and the resulting residuals (*bottom*). See Table 1 for the model parameters.

Clearly, the modest energy resolution of *ROSAT* does not allow us to distinguish among several models that could describe the spectral structure present in the data. We summarize these models in Table 1. In all cases, the residuals appear nearly identical to these for the absorbed power-law + edge model as discussed above. The Galactic N_H is only 4.55×10^{20} cm^{-2} (Elvis, Lockman, & Wilkes 1989), so regardless of their interpretation of the edge, there is a rather substantial amount of cold intrinsic absorption in the line of sight to IC4329A (as expected given the edge-on orientation of the galaxy; see Petre et al. 1984 for details). We note here that this intrinsic cold absorption is neglected by Nandra & Pounds (1994) in their fit to the *Ginga* spectrum of IC 4329A, yielding a larger ionized column than that inferred here. Regardless of the model, the 0.1–2 keV flux of from IC 4329A is 3×10^{-11} ergs cm^{-2} s^{-1}, with a nominal $\sim 10\%$ error due to the absolute effective area calibration uncertainties. The unabsorbed 0.1–2 keV flux (at $\alpha = 1$) varies markedly between the different models, from 8×10^{-11} (partial covering), 1.7×10^{-10} (ionized absorber), and 7×10^{-10} (blackbody) ergs cm^{-2} s^{-1}, respectively. With the ionized absorber, this corresponds to a luminosity of 1.8×10^{44} ergs s^{-1} ($H_0 = 50$ km s^{-1} Mpc^{-1}).

3.1.2. *OSSE Spectrum of IC 4329A*

The spectral fit parameters to the OSSE data alone during viewing period 207 differ only slightly (except for the flux, which is now greater by a factor of 4) from those reported in F93. We have used the data up to ~ 1 MeV, as the upper limits for higher energies are above predictions of any plausible model and inclusion of the higher energy data only increases statistical noise. Signal is detected up to ~ 200 keV. A simple power-law model fits the data adequately and yields $\alpha = 1.61^{-0.33}_{+0.38}$ with $\chi^2 = 123/117$ d.o.f. The normalization of the power law at 100 keV is $(5.4 \pm 0.4) \times 10^{-3}$ photons cm^{-2} s^{-1} MeV^{-1}. The limits ($\Delta\chi^2 = 3.84$) on the strength of a Gaussian 511 keV line vary from 4.8 to 10×10^{-5} photons cm^{-2} s^{-1} for the line widths from 5 keV to 350 keV.

The co-added spectrum for all three viewing periods is virtually identical to that of the period 207; the best-fit power-law index is $\alpha = 1.60 \pm 0.25$, and the 100 keV normalization is $(4.9 \pm 0.3) \times 10^{-3}$ photons cm^{-2} s^{-1} MeV^{-1}, which yields $\chi^2 = 58/51$ d.o.f. Both normalizations are consistent with each other within the statistical uncertainties.

3.1.3. *Joint ROSAT/OSSE Spectrum of IC 4329A*

We then fitted both simultaneous data sets jointly (with the same model normalization). We used a model consisting of an underlying power law with an exponential cutoff at E_C ($F_E \propto E^{-\alpha} e^{-E/E_C}$) plus reflection, uniform neutral absorption, and an absorption edge. Due to the gap in the data between 2 and 50 keV, the normalization, f_r, of the reflection component is only poorly constrained. Our model reflection spectrum is that of Lightman & White (1988) which calculates the average spectrum seen over all inclinations for an isotropic source illuminating a solar abundance flat slab of material. Then the value of $f_r = 1$ corresponds to an inclination of $\sim 60°$, while a face-on

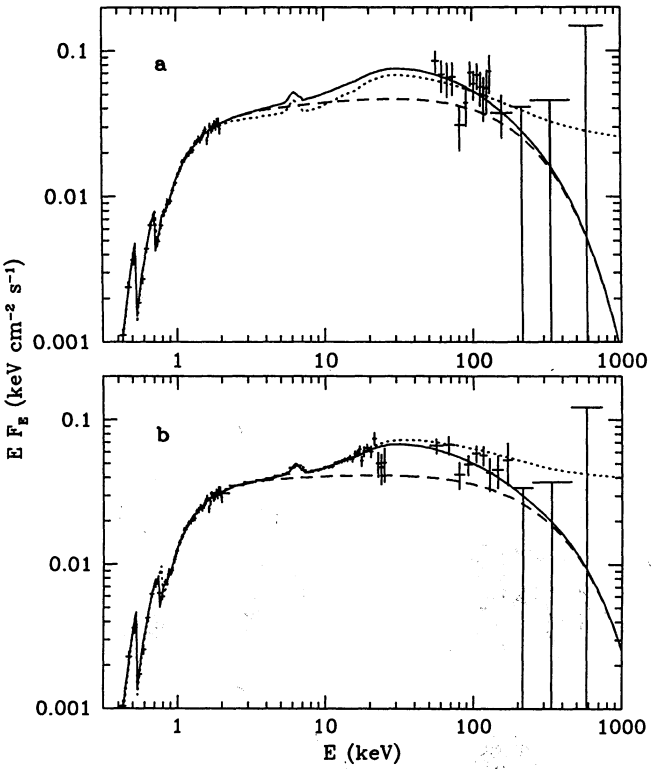

FIG. 4.—The broad-band spectrum (in EF_E) of IC 4329A. The crosses give the data, the solid curves represent the best-fit power law with an exponential cutoff, reflection, Fe K line, and absorption (see Table 1, models A, D, for parameters); the dashed curves represent the power-law component with the cutoff but without the contribution from reflection. It is apparent that the reflection contribution is important in the OSSE energy range. For comparison, the dotted curves show the best-fit spectrum for the model without the cutoff. The upper limits are 2 σ. (*a*) The *ROSAT* (<2 keV) and OSSE (>50 keV) data. One sees that both models with and without the exponential cutoff are compatible with the data, which is possible due to a change in the spectral index (see Table 1). (*b*) The data including the nonsimultaneous *Ginga* data (2–25 keV) and the sum of all OSSE observations of IC 4329A. The model without the cutoff is ruled out as the spectral index is fixed by the *Ginga* data.

view gives $f_r = 1.33$ (Ghisellini, Haardt, & Matt 1994). Uncertainties in geometry lead us to constrain $1 \leq f_r \leq 2$: the *Ginga* data (F92; see below) show the amount of reflection to lie in the middle of this range. The best fit to the OSSE data is then shown by the solid curve in Figure 4*a*; its parameters are given in Table 2 (model A). We find that a cutoff in the underlying power law is *not* required as the model without a cutoff (*dotted curve*) gives $\Delta\chi^2 = 2.6$ (for $\alpha = 1.07$ and $f_r = 2$). The relative steepness of the OSSE data can be thus entirely explained by the contribution from the steep high-energy component of reflection, without the necessity of an intrinsic spectral break. The EGRET limit implies $E_C \gtrsim 300$ MeV only (for the sum of all EGRET observations).

3.1.4. *Joint ROSAT/Ginga/OSSE Spectrum of IC 4329A*

As discussed above, two past *Ginga* observations have the 2 keV flux identical to that of our *ROSAT* observation. We used those data to construct composite broad-band spectra, which then constrain the spectral parameters much more tightly than the *ROSAT*/OSSE data alone. In particular, they do show the presence of a high-energy break in the underlying spectrum. We stress, however, that these composite spectra are less certain than those from *ROSAT*/OSSE alone. In particular, a small change in α from the value seen by *Ginga* can strongly affect the value of E_C.

We have used the *Ginga* data up to 25 keV in our analysis. While including the data above 20 keV might result in a small increase in the overall χ^2 because of the possibility of contamination by the instrumental silver line at 22–25 keV, these data are of relatively low statistical weight. We therefore do not expect this contamination to affect the derived spectral parameters significantly. Nonetheless, to allow for the residual calibration uncertainties, we added in quadrature to the statistical errors a 1% systematic error in the count rate in each PHA channel. Following Piro et al. (1990) and F92, we modeled the data as an absorbed power law with Compton reflection and a Gaussian Fe Kα line. For the observations on 1989 July 8 and 9, we obtained $\alpha = 0.97 \pm 0.06$ and $1.03^{+0.25}_{-0.06}$, $N_H = (4.6 \pm 1.3)$ and $(5.0 \pm 1.4) \times 10^{21}$ cm^{-2}, $f_r = 1.06^{+0.41}_{-0.34}$ and 1.33 ± 0.48, the Fe line energy of $E_{Fe} = 6.21 \pm 0.17$ and $6.14^{+0.31}_{-0.39}$ keV, the line flux of $I_{Fe} = (1.34^{+0.50}_{-0.39})$ and $(1.36^{+1.18}_{-0.58}) \times 10^{-4}$ photons s^{-1} cm^{-2} (corresponding to an equivalent width of $\sim$135 eV), and χ^2/d.o.f. of 23/28 and 21/28, respectively.

We then fitted the data sets for the three instruments jointly (with the same model normalization). We used the same model as in the *ROSAT*/OSSE fit but now with addition of an iron line. The parameters of the fit are given in Table 2. We have found little difference in the best-fit parameters whether using the *Ginga* data of July 8 (model B) or 9 (model C). The total absorbed 0.1–1000 keV X-ray/γ-ray luminosity for model B is 5×10^{44} ergs s^{-1}. As seen from Table 2, the addition of the *Ginga* data constrains α and f_r much more tightly than the *ROSAT*/OSSE data alone. As a consequence, the cutoff energy is also constrained more tightly, between 250 and 1700 keV (models B and C). The model without cutoff (and with reflection) gives $\Delta\chi^2 \simeq 22$ and 8, for models B and C, respectively. Although these model spectra fit the data below 200 keV, they are, however, above the upper limits in the 200–500

TABLE 2

PARAMETERS FOR THE JOINT FITS

Model	N_H (10^{21} cm^{-2})	E_{edge} (keV)	τ_{edge}	E_{Fe} (keV)	σ_{Fe} (keV)	I_{Fe} (10^{-4} photons s^{-1} cm^{-2})	α	E_C (keV)	f_r	χ^2/d.o.f.
A.....	$3.0^{+0.5}_{-0.3}$	0.72 ± 0.05	$0.57^{+0.20}_{-0.16}$	...	...	...	$0.86^{+0.21}_{-0.13}$	$220^{+\infty}_{-110}$	1^{+1}_{-0}	153/159
B.....	3.2 ± 0.2	0.75 ± 0.04	$0.60^{+0.17}_{-0.14}$	$6.20^{+0.17}_{-0.2}$	0.33 ± 0.33	$1.33^{+0.49}_{-0.38}$	0.94 ± 0.03	370^{+270}_{-120}	$1.03^{+0.26}_{-0.24}$	178/191
C.....	3.4 ± 0.2	0.76 ± 0.04	0.62 ± 0.15	$6.10^{+0.27}_{-0.40}$	$0.59^{+0.57}_{-0.59}$	$1.31^{+0.91}_{-0.54}$	0.98 ± 0.04	610^{+1100}_{-270}	$1.17^{+0.36}_{-0.30}$	181/191
D.....	3.2 ± 0.2	0.75 ± 0.04	$0.60^{+0.17}_{-0.14}$ *	$6.20^{+0.17}_{-0.2}$	$0.33^{+0.47}_{-0.33}$	$1.32^{+0.48}_{-0.38}$	0.93 ± 0.03	320^{+150}_{-80}	$1.04^{+0.26}_{-0.23}$	109/125
E.....	3.4 ± 0.2	0.76 ± 0.04	$0.63^{+0.18}_{-0.13}$	$6.10^{+0.28}_{-0.34}$	$0.59^{+0.57}_{-0.59}$	$1.31^{+0.90}_{-0.53}$	$0.98^{+0.04}_{-0.03}$	480^{+420}_{-160}	$1.18^{+0.34}_{-0.30}$	113/125

NOTE.—Errors are given for $\Delta\chi^2 = 2.7$.

[a] A: simultaneous *ROSAT*/OSSE data only, $1 \leq f_r \leq 2$; B/D and C/E: including *Ginga* data for 1989 July 8 and 9, respectively; D/E: OSSE data for the sum of all observations used.

keV range. Still, as the *Ginga* observations were not simultaneous with those of *ROSAT* and OSSE, we have to consider the evidence for a high-energy break as only tentative. To settle this issue, simultaneous *ASCA* and OSSE (or XTE) observations are necessary.

To aid our understanding of the existence of a cutoff in the spectrum before such observations, we have also used the sum of all the OSSE observations (§§ 2.2, 3.1.2). OSSE has detected no spectral variability in IC 4329A, which justifies using the average spectrum. Repeating fits for the OSSE sum we get results given in Table 2, models D, E. There is almost no change in the parameters except that we can constrain E_C even tighter, between 240 and 900 keV. The decreased upper limit on E_C is due to the decreased flux upper limits above 200 keV. Figure 4*b* shows the spectrum for the model D.

Figure 5 shows the corresponding residuals for the model D. We see that the model is adequate for all three instruments. We get χ^2 per number of PHA channels of 31/47, 22/35, and 55/53, which values are almost identical to those for the best fits for the individual instruments separately.

3.2. *Spectrum of the Elliptical Galaxy IC 4329 and the Source S3*

The *ROSAT* data for the companion galaxy, IC 4329, were fitted in an analogous manner. Here we find that a Raymond & Smith (1976) plasma model (with solar abundances) fits reasonably well ($\chi^2 = 14/17$ d.o.f.), with a temperature $kT = 0.87 \pm 0.11$ keV, absorbed by a column of $2.8^{+4.0}_{-1.2} \times 10^{20}$ cm^{-2}, entirely consistent with the absorption due to our own Galaxy of 4.55×10^{20} cm^{-2} (measured toward IC 4329A by Elvis, Lockman, & Wilkes 1989, but should not be different by more than a few percent within 3′). The corresponding 0.1–2 keV flux is 6.5×10^{-13} ergs cm^{-2} s^{-1}. At $z = 0.0157$, the corresponding luminosity is 6.8×10^{41} ergs s^{-1}, rather average-to-high for its class (Fabbiano, Kim, & Trinchieri 1992). We cannot place any better limits on abundances than $0.2 < A < 3$. We note here that this object was detected with the *Einstein Observatory* HRI (Fabbiano et al. 1992), but that this is the first time its spectral parameters can be measured.

Similarly, we fitted the data for the source S3. We find that an absorbed power law, with a column of $3.1^{+2.0}_{-1.7} \times 10^{20}$ cm^{-2} and a spectral index $\alpha = 1.3^{+0.7}_{-0.6}$, fits the data well ($\chi^2 = 8.5/17$ d.o.f.); again, the absorption is entirely consistent with the Galactic value. The 0.1–2 keV flux is 8.7×10^{-13} ergs cm^{-2} s^{-1}. To the best of our knowledge, this source has not previously appeared as a serendipitous object (e.g., there were no *Einstein Observatory* Imaging Proportional Counter observations of the field of IC 4329A). Judging by its X-ray spectrum and the high Galactic latitude, it is likely to be an AGN. However, there are no sources listed in the Véron quasar catalog within 5′ of its X-ray position.

The *ROSAT* spectra and the measured fluxes for both IC 4329 and S3, which over the full *ROSAT* PSPC bandpass are substantially lower than that of IC 4329A, imply that it is unlikely that either object has substantially contaminated the OSSE data, or any previously measured spectra of IC 4329A, obtained with collimated proportional counter instruments as the *Ginga* LAC or *EXOSAT* ME. That is because these instruments are sensitive above 1 keV, where the flux from IC 4329A dominates by at least a factor of 10. However, around ~0.4 keV, the fluxes of all three objects are comparable, and below ~0.3 keV, IC 4329A is the faintest (see Fig. 6), primarily because its spectrum is more heavily absorbed that the other two sources.

4. CONCLUSIONS

The most important result of this paper is that the spectrum of IC 4329A is compatible with a single power law modified by absorption and reflection extending from soft X-rays to soft γ-rays. The evidence for a spectral break in γ-rays from the simultaneous *ROSAT*/OSSE data is weak, with only a constraint of $E_C \gtrsim 100$ keV. A break between ~250 keV and ~1700 keV would be required if the simultaneous spectrum in the 2–20 keV range were similar to that from the earlier *Ginga* observations, which have the 2 keV flux in excellent agreement

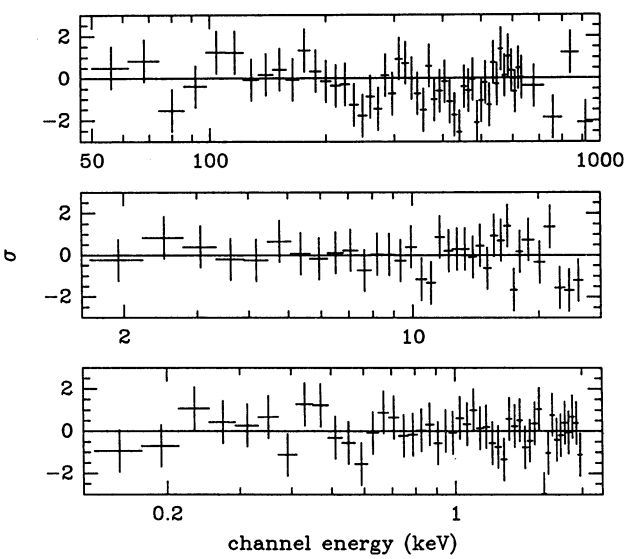

FIG. 5.—The unbinned residua of the best fit shown in Fig. 1*b*, for *ROSAT*, *Ginga*, and OSSE, from bottom to top, respectively. It is apparent that the agreement of the raw data with the model is excellent. The lack of significant residuals above 200 keV (where no signal is detected) shows the level of accuracy of the background subtraction.

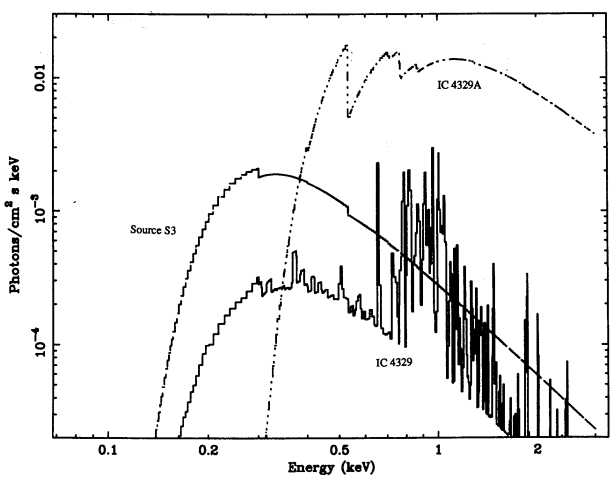

FIG. 6.—The best-fitting spectral models for the three brightest sources (IC 4329A, IC 4329, and S3) present in the *ROSAT* field of view. While IC 4329A is by far the strongest source above 0.5 keV, the other two sources, if not spatially resolved, could provide significant flux contamination below 0.3 keV.

with that seen by *ROSAT*. In any case, the break is at a higher energy than both observed in NGC 4151 ($E_C \sim 50$ keV: Maisack et al. 1993; Zdziarski et al. 1993), and thought before to be typical for Seyfert 1s (F93).

In addition, our *ROSAT* data show that the low-energy spectrum is complex, with significantly higher absorption than expected from the column in our own Galaxy. At least a part of this excess absorption ($\sim 3 \times 10^{21}$ cm^{-2}) is likely to be due to cold material, expected from the nearly edge-on orientation of the host galaxy. In addition, there is additional structure in the soft X-ray spectrum, although the modest energy resolution of the PSPC cannot differentiate between an ionized absorber, partial covering by neutral material, or a soft excess.

Further theoretical consequences of this observation are studied in Zdziarski et al. (1994). In that paper, it is shown that the underlying hard X-ray power law can be adequately described by either optically thin ($0.02 \lesssim r \lesssim 0.5$) thermal Comptonization, where the scattering medium is mildly relativistic (100 keV $\lesssim kT \lesssim$ 500 keV), or, alternatively, by nonthermal models. In the later case, the lack of a strong (direct or down-scattered) annihilation line in the data requires that electron injection must be at relatively low energies; this can be accomplished when the electron injection is either monoenergetic at a low electron Lorentz factor, $\gamma \sim 3$, or a steep power law extending down to the minimum $\gamma \lesssim 10$. In all cases, the reflection *is required*. Even though the *Ginga* observations alone allow the "hard tail" to be due to partial covering of the source (but with the column density of $\sim 2.4 \times 10^{24}$ cm^{-2}, about two orders of magnitude greater than would be implied by the spectral structure in the *ROSAT* data), the broad ($\sigma > 0.3$ keV), strong (EW > 100 eV) Fe Kα line (cf. Done 1994) independently implies the presence of the reflecting medium.

This research has been supported in part by NASA grants NAG5-2439, NAGW-3129, and NAG5-1813, and the Polish KBN grant 221129102. A. C. F. and A. C. acknowledge the Royal Society and K. N. acknowledges the SERC for financial support.

APPENDIX

CONSIDERATION OF THE PSPC INSTRUMENTAL EFFECTS

We considered if it is possible that the edgelike feature is only an artifact of the instrumental effects and, in particular, of miscalibration of the PSPC that would manifest itself as an erroneous resolution matrix. Two such matrices were generated for analysis of the PSPC data: the early version, the "92 Mar 11" matrix, and the current version, used in all the analysis above, the "93 Jan 12" matrix. Specifically, we wanted to verify that the fit parameters are only weakly affected by the choice of matrix, and if the confidence region on the fit parameters overlap. To that end, we prepared a PSPC data set *without* the 2% systematic error added, to make sure that we would not unnecessarily increase the error ranges on the fit parameters (as opposed to the data set used in all previous fitting, which included this 2% error). We then fitted the *ROSAT* data with both matrices, using two of the models considered in § 3.1: absorbed power-law and absorbed power-law with an edge ~ 0.7 keV.

The results are summarized in Table 3. It is clear that the improvement in χ^2 is significant regardless of the resolution matrix used, and that the errors on all parameters overlap for fits using both PSPC resolution matrices. We thus conclude that if the differences between the parameters inferred by the use of the two PSPC resolution matrices represent adequately the systematic error in the spectral fits, the parameters of the continuum and the inferred oxygen edge as given in § 3.1.1 are a good description of the data.

TABLE 3

DEPENDENCE OF THE *ROSAT* SPECTRAL FIT PARAMETERS ON THE ADOPTED PSPC RESOLUTION MATRIX

Model	N_H (10^{21} cm^{-2})	α	E_{edge} (keV)	τ_{edge}	χ^2/d.o.f.
Current ("93 Jan 12") PSPC Resolution Matrix					
Absorbed power-law	2.1 ± 0.3	0.16 ± 0.17	...	...	54.2/44
Absorbed power-law plus edge.....	3.0 ± 0.7	$0.84^{+0.41}_{-0.37}$	$0.72^{+0.06}_{-0.07}$	0.56 ± 0.21	34.9/42
"92 Mar 11" PSPC Resolution Matrix					
Absorbed power-law	1.9 ± 0.3	0.19 ± 0.16	...	...	58.6/44
Absorbed power-law plus edge.....	3.4 ± 0.8	1.14 ± 0.45	0.76 ± 0.05	0.62 ± 0.23	37.5/42

NOTE.—See the Appendix for details.

REFERENCES

Done, C., 1994, preprint
Done, C., Mulchaey, J. S., Mushotzky, R. F., & Arnaud, K. A. 1992, ApJ, 395, 275
Elvis, M., Lockman, F. J., & Wilkes, B. J. 1989, AJ, 97, 777
Fabbiano, G., Kim, D. W., & Trinchieri, G. 1992, ApJS, 80, 531
Fabian, A. C., Nandra, K., Celotti, A., Rees, M. J., Grove, J. E., & Johnson, W. N. 1993, ApJ, 416, L57 (F93)
Fiore, F., Perola, G. C., Matsuoka, M., Yamauchi, M., & Piro, L. 1992, A&A, 262, 37 (F92)
Ghisellini, G., Haardt, F., & Matt, G. 1994, MNRAS, 267, 743
Halpern, J. 1982, Ph.D. thesis, Harvard Univ.
Kallman, T., & McCray, R. 1982, ApJS, 50, 263
Krolik, J. H., & Kallman, T. 1992, NASA/Goddard preprint
Lightman, A. P., & White, T. R. 1988, ApJ, 335, 57
Maisack, M., et al. 1993, ApJ, 407, L61
Nandra, K., & Pounds, K. 1992, Nature, 359, 215
———. 1994, MNRAS, 268, 405
Petre, R., Mushotzky, R. F., Krolik, J., Holt, S. S. 1984, ApJ, 280, 499
Piro, L., Yamauchi, M., & Matsuoka, M. 1990, ApJ, 360, L35
Pounds, K. A., Nandra, K., Stewart, G. C., George, I. M., & Fabian, A. C. 1990, Nature, 344, 132
Raymond, J. C., & Smith, B. H. 1976, ApJS, 35, 419
Wilson, A. S., & Penston, M. V. 1979, ApJ, 232, 389
Yaqoob, T., Warwick, R. S., Makino, F., Otani, C., Sokoloski, J. L., Bond, I. A., & Yamauchi, M. 1993, MNRAS, 262, 435
Zdziarski, A. A., Fabian, A. C., Nandra, K., Celotti, A., Rees, M. J., Done, C., Coppi, P. S., & Madejski, G. M. 1994, MNRAS, 269, L55
Zdziarski, A. A., Lightman, A. P., & Maciołek-Niedźwiecki, A. 1993, ApJ, 414, L93